Common-Reflection-Surface (CRS) approaches for stacking of 3-D seismic data

Pedro Chira-Oliva(*) and João Carlos R. Cruz(*), Department of Geophysics, UFPA, Brazil,
(*)chira,jcarlos@ufpa.br

This paper was prepared for presentation at the 9th International Congress of the Brazilian Geophysical Society held in Salvador, Brazil, 11-14 September 2005.

Abstract

The Common-Reflection-Surface (CRS) stack is a macro-model independent seismic imaging method that, in many important situations, improve the imaging quality with respect to the conventional methods (e.g. Normal-Moveout/Dip-Moveout (NMO/DMO) stack). The CRS method has been sucessfully applied both 2-D synthetic and real seismic data. Recently, it was also tested for full and narrow azimuth 3-D data with satisfactory results, showing its advantages over conventional methods. By using optimized search strategies, the CRS parameters are estimated by means of a coherence analysis procedure. The estimated 3-D CRS parameters (fourteen parameters for the finite-offset (FO) central ray and eight parameters for the zero-offset (ZO) central ray) are used in the hyperbolic traveltime approach to stack the 3-D multi-coverage seismic data, providing as results a high-resolution simulated FO or ZO volume, and coherence and parameter volumes. The 3-D CRS approach is also specialized in order to approximate diffraction traveltimes. In this case the central ray is a diffraction ray, and the stack formalism depends on ten parameters (FO case) and five parameters (ZO case). In this work, we present the formalism and examples of applications of the 3-D CRS stacking operator for reflection and diffraction events. We consider two cases for the central ray, ZO and FO, respectively. We show special formulas for applications of the 3-D CRS attributes to determine, e.g. the geometrical spreading (GS) factor and projected Fresnel zones, important to define the aperture for stacking and migration.

Introduction

The essence of the 3-D seismic method is an areal data collection followed by processing and interpretation of the data volume. 3-D surveys provide more details of the subsurface and contribute significantly to the problems of field appraisal, development, production and exploration. The fundamental objective of the 3-D seismic method is an increased resolution. Likely the 2-D seismic method, the ZO seismic volume is obtained by stacking an ensemble of seismic traces following a hyperbolic reflection traveltime approach. The conventional 3-D ZO seismic stack suffers from the same limitations that occur by using the 2-D Normal-moveout/Dip-moveout (NMO/DMO) stack method, e.g, strong dependence on velocity analysis, conflicting dip problems, effects due to pulse stretch and asymmetric acquisition geometry.

In order to overcome limitations of the NMO/DMO method, as so as to improve seismic imaging results, so-called model-independent methods have been introduced (Hubral, 1999). The Common-Reflection-Surface (CRS) stack (e.g., Mann et al., 1999, Jäger et al., 2001; Garabito et al., 2001) is one of these new methods. For a survey on model-independent methods, the reader is referred to Hubral (1999). The CRS method formalism is based on the second-order hyperbolic paraxial traveltime approximation in the vicinity of a central ray. In the FO case, the central ray is an arbitrary offset ray. In the ZO case the central ray is a normal ray. For a full azimuth 3-D dataset, this approximation depends on fourteen parameters (FO case) and eight parameters (ZO case). For a narrow azimuth 3-D dataset, the number of parameters reduces to seven (FO case) and six or four (ZO case). The first successful results of the 3-D CRS stack applied to synthetic dataset were shown by Cristini et al. (2001). Interesting examples of 3-D CRS stack for real data were shown by Cristini et al. (2002) and Bergler et al. (2002). This method is very efficient in case of strong lateral velocity variations, structural complexity, poor signal-to-noise ratio (S/N) and low fold coverage data. Under the assumption of a spherical normal-incidence-point (NIP) wavefront at the surface, this method was applied for 3-D datasets with narrow-azimuth acquisitions (Cardone et al., 2003). The results were an improved stacking section and an improved stacking velocity analysis with respect to conventional techniques. Cristini et al. (2003) showed that the 3-D ZO CRS stack method gives high resolution imaging even in case of low S/N data and in the presence of complex structures in real dataset.

In this paper, we present the 3-D CRS stack method in the framework of its application to construct a simulated FO or ZO volume by a stacking procedure carried out on a 3-D pre-stack seismic dataset. We extend the 3-D CRS traveltime approximation or stacking operator to consider diffractions events. We also present some applications that result from the knowledge of the estimated 3-D CRS parameters for FO (fourteen parameters) and ZO (eight parameters) cases, respectively.

3-D CRS stacking operators

Reflection events

We consider an arbitrary 3-D inhomogeneous layered medium separated by smooth and curved interfaces. The measurement surface is planar and horizontal, z=0 (Figure 1). It is considered a fixed primary reflection ray, called the central ray. This ray connects a source at point *S* and a receiver at point *G*. In the vicinity of *S* and *G*

points we define the initial and end points, $\overline{S}$ and $\overline{G}$. The ray that links these points, $\overline{S}$ and $\overline{G}$, is called paraxial ray (Figure 1a). For the case of a normal (central) ray, the source and receiver are coincident at point X_0 (Figure 1b).

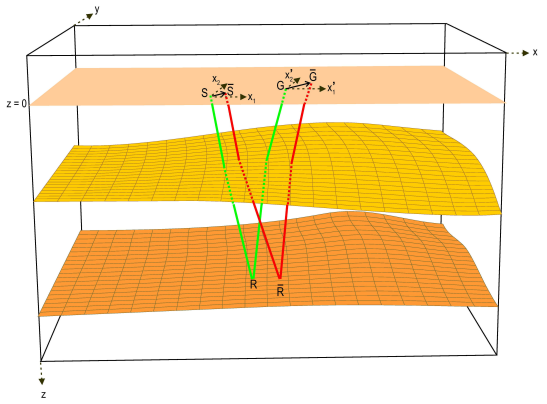

(a)

(b)

Figure 1. 3-D model constituted of two isovelocity layers separated by smooth and curved interfaces above a half-space. a) For the case of a FO (central) ray, *SRG* (green line), we consider two local Cartesian coordinates system, one centered at point *S* and defined by (x_1,x_2) and other centered at point *G* and defined by (x_1',x_2'). b) For a ZO (central) ray (green line), we consider one local Cartesian coordinates system centered at point X_0 and defined by (x_1,x_2). The paraxial ray $\overline{S}\overline{R}\overline{G}$ is depicted in red line.

On the planar and horizontal measurement surface we define two 2-D local Cartesian coordinate systems, $\mathbf{x}(x_1,x_2)$ and $\mathbf{x}'(x_1',x_2')$, with origins at the initial and end point of the central ray *SG* (Figure 1a). For a normal (central) ray, the origin is the point X_0. It is used to locate all sources and receivers of the paraxial rays, $\mathbf{s} = (x_S,y_S)$ and $\mathbf{g} = (x_G,y_G)$, on the surface (see Figure 2). The vector **s** represents the dislocation vector between the sources of the paraxial and central ray. It is analogous for the vector **g**. Source and receiver pairs can be conveniently located by means of midpoint and half-offset coordinates, $(\mathbf{x_m},\mathbf{h})$, defined by $\mathbf{x_m} = (1/2)(x_G + x_S, y_G + y_S)$ and $\mathbf{h} = (1/2)(x_G - x_S, y_G - y_S)$. It is also defined a global Cartesian coordinate system by (x,y,z). The depth is given by the axis z.

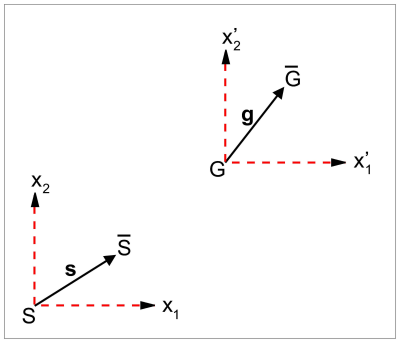

(a)

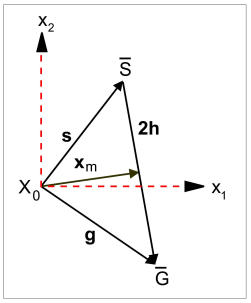

(b)

Figure 2. Local Cartesian coordinate systems, a)FO case: The initial and end points of the central ray are defined by *S* and *G* and for the paraxial ray are denoted by $\overline{S}$ and $\overline{G}$. The vectors **s** and **g** denote the dislocation vector between *S* and $\overline{S}$ and *G* and $\overline{G}$. b)ZO case: The shot and receiver vectors originated at the point X_0 are denoted by **s** and **g**. The vectors $\mathbf{x_m}$ and **h** denote the midpoint and half-offset vectors on the planar and horizontal measurement surface (z=0).

Finite-Offset (FO) case - For this case, the source and receiver of the central ray are not coincident, and the 4x4 surface-to-surface propagator matrix **T** associated to the FO (central) ray, is given by

$$\mathbf{T} = \begin{pmatrix} \underline{\mathbf{A}} & \underline{\mathbf{B}} \\ \underline{\mathbf{C}} & \underline{\mathbf{D}} \end{pmatrix}, \qquad (1)$$

where $\underline{\mathbf{A}}$, $\underline{\mathbf{B}}$, $\underline{\mathbf{C}}$ and $\underline{\mathbf{D}}$ denote 2x2 matrices (e.g., Bortfeld, 1989; Hubral et al., 1992; Schleicher et al., 1993b).

The 3-D FO CRS hyperbolic traveltime approximation in the vicinity of an arbitrary (central) ray (Schleicher et al., 1993a; Jäger, 1999) is defined by (with a modified notation)

$$t_{FO}^2(\mathbf{x}_m,\mathbf{h}) = \left(t_1 + \mathbf{p}_m \cdot \mathbf{x}_m + p_h \cdot \mathbf{h}\right)^2 + t_1\left(\mathbf{x}_m \cdot \mathbf{M_1} \mathbf{x}_m + 2\mathbf{x}_m \mathbf{M_2} \mathbf{h} + \mathbf{h} \cdot \mathbf{M_3} \mathbf{h}\right), \quad (2)$$

where

$$\mathbf{p}_h = \frac{\partial t_{FO}}{\partial \mathbf{h}} = \mathbf{p}_S + \mathbf{p}_G, \quad (3a)$$

$$\mathbf{p}_m = \frac{\partial t_{FO}}{\partial \mathbf{x}_m} = \mathbf{p}_G - \mathbf{p}_S, \quad (3b)$$

$$\mathbf{M_1} = \frac{\partial^2 t_{FO}}{\partial \mathbf{x}_m^2} = \mathbf{N}_S^G + \mathbf{N}_G^S - \mathbf{N}_{SG}^T - \mathbf{N}_{SG}, \quad (4)$$

$$\mathbf{M_2} = \frac{\partial^2 t_{FO}}{\partial \mathbf{h} \partial \mathbf{x}_m} = -\mathbf{N}_S^G + \mathbf{N}_G^S + \mathbf{N}_{SG}^T - \mathbf{N}_{SG}, \quad (5)$$

$$\mathbf{M_3} = \frac{\partial^2 t_{FO}}{\partial \mathbf{h}^2} = \mathbf{N}_S^G + \mathbf{N}_G^S + \mathbf{N}_{SG}^T + \mathbf{N}_{SG}, \quad (6)$$

being $\mathbf{p}_m$ and $\mathbf{p_h}$ the midpoint and half-offset slowness coordinates, respectively. The vectors $\mathbf{p}_S$ and $\mathbf{p}_G$ denote the projections of the slowness vectors of the central ray at points *S* and *G*, into planar measurement surface. The 2x2 second-derivative matrices of the traveltime t_{FO} with respect to midpoint and half-offset coordinates are represented by $\mathbf{M_1}$, $\mathbf{M_2}$ and $\mathbf{M_3}$. The matrix $\mathbf{N}_G^S$ (respectively $\mathbf{N}_S^G$) is the point-source matrix at *G* (respectively at *S*), evaluated at $\mathbf{s} = \mathbf{0}$, i.e. a point source at *S* (respectively $\mathbf{g} = \mathbf{0}$, i.e. a point receiver at *G*). These matrices $\left(\mathbf{N}_G^S, \mathbf{N}_S^G\right)$ are (symmetric) second-derivate matrices of the traveltime t_{FO}. The matrix $\mathbf{N}_{SG}$ is the second-order mixed-derivate matrix of the traveltime t_{FO}. It is, in general, non-symmetric (Schleicher et al., 1993a). Here, t_1 denotes the traveltime along the FO (central) ray. The 3-D FO CRS operator (equation 2) depends on fourteen parameters: three parameters from (symmetric) matrix $\mathbf{M_1}$, four parameters from (non symmetric) matrix $\mathbf{M_2}$, three parameters from (symmetric) matrix $\mathbf{M_3}$, two from vector $\mathbf{p}_h$ and two from vector $\mathbf{p}_m$.

According to Hubral et al. (1992b) the central ray *SG* can be subdivided into two ray branches *SM* and *MG*. These are characterized by the two surface-to-surface ray-branch propagator matrices $\mathbf{T_1}$ and $\mathbf{T_2}$. The point *M* results cutting the central ray *SG* from an arbitrary curved smooth surface (e.g. a reflecting/transmitting interface, etc). These matrices satisfy the so-called chain rule, $\mathbf{T} = \mathbf{T_2}\,\mathbf{T_1}$.

Zero-Offset (ZO) case - For this case, the source and receiver of the central ray are coincident, being denoted by X_0. The central ray becomes a normal ray that is perpendicular to the reflector (see Figure 1b). The traveltime of the normal or ZO (central) ray is denoted by t_0.

The hyperbolic paraxial traveltime approximation in the vicinity of a normal (central) ray can be expressed by (Schleicher et al., 1993a)

$$t_{ZO}^2(\mathbf{x}_m,\mathbf{h}) = \left(t_0 + 2\mathbf{p}_0 \cdot \mathbf{x}_m\right)^2 + 2t_0 \mathbf{x}_m \cdot \mathbf{D}_0^{-1}\mathbf{C}_0 \mathbf{x}_m + \mathbf{2t}_0 \mathbf{h} \cdot \mathbf{B}_0^{-1}\mathbf{A}_0 \mathbf{h}, \quad (7)$$

Here, $\mathbf{p_0} = (\partial t/\partial \mathbf{x}_m)/2$ is the horizontal projection of the slowness vector of the normal (central) ray at X_0 onto the measurement surface. The "·" denotes the scalar product. Moreover,

$$\mathbf{D}_0^{-1}\mathbf{C}_0 = \frac{1}{2}\frac{\partial^2 t}{\partial \mathbf{h}^2} \quad \text{and} \quad \mathbf{B}_0^{-1}\mathbf{A}_0 = \frac{1}{2}\frac{\partial^2 t}{\partial \mathbf{x}_m^2}, \quad (8)$$

are 2x2 second-order derivative (Hessian) matrices also evaluated at X_0. We recall that $\mathbf{A_0}$ $\mathbf{B_0}$, $\mathbf{C_0}$ and $\mathbf{D_0}$ represent the (constant) 2x2 submatrices of the 4x4 propagator matrix $\mathbf{T_0}$ of the one-way normal ray, that starts at the normal-incidence-point (NIP) of the central ray and reaches the measurement surface at X_0 (Bortfeld, 1989; Hubral et al., 1992a, see Figure 1b). By introducing the notation $\mathbf{D_0^{-1}C_0} = \mathbf{A}/v_1$, $\mathbf{B_0^{-1}A_0} = \mathbf{B}/v_1$ and $\mathbf{p_0} = \mathbf{c}/v_1$, we obtain (e.g. Chira, 2003; Chira-Oliva et al., 2003)

$$t_{ZO}^2(\mathbf{x}_m,\mathbf{h}) = \left(t_0 + \frac{2}{v_1}\mathbf{c} \cdot \mathbf{x}_m\right)^2 + \frac{2t_0}{v_1}\left[\mathbf{x}_m \cdot \mathbf{A}\mathbf{x}_m + \mathbf{h} \cdot \mathbf{B}\mathbf{h}\right], \quad (9)$$

where v_1 is the medium velocity at X_0.

Following Hubral et al. (1991) and Chira (2003) we can also write

$$\mathbf{A} = \mathbf{D}_{zy}\mathbf{N}\mathbf{D}_{zy}^T \quad \text{and} \quad \mathbf{B} = \mathbf{D}_{zy}\mathbf{M}\mathbf{D}_{zy}^T, \quad (10)$$

where $\mathbf{D}_{zy}$ is the 2-D transformation matrix (Jäger, 1999)

$$D_{zy} = \begin{pmatrix} \cos j_1 \cos j_2 & -\sin j_1 \\ \sin j_1 \cos j_2 & \cos j_1 \end{pmatrix}, \quad (11)$$

M and **N** are symmetric 2x2 curvature matrices of the Normal-Incidence-Point (NIP) and Normal (N) waves (Hubral, 1983)). The 3-D ZO CRS stacking operator (equation 9) depends on eight parameters: three parameters from (symmetric) matrix **A**, three parameters from (symmetric) matrix **B** and two from vector **c**. The superscript *T* denotes transposition. The symmetric 2x2 matrices **A** and **B** represent the second-order derivatives of the traveltime t_{ZO} with respect to midpoint and half-offset coordinates times the velocity v_1. The ground surface projection vector of the normal ray at X_0 is denoted by **c**. The azimuth and polar angle of the normal ray direction are described by φ_1 and φ_2, respectively.

Diffraction events

One of the important problems in the interpretation of seismic data is the identification of structural geologic feature (e.g. faults, small-size scattering object). Local elements in the subsurface with a size comparable to the source wavelength are usually ignored by processing and are identified only during the interpretation process (Landa et al., 1987).

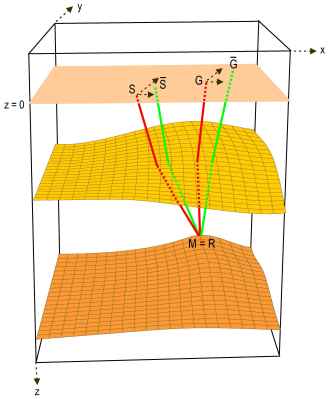

Figure 3. 3-D model constituted of two isovelocity layers separated by smooth and curved interfaces above a half-space. For a diffraction point, the depth point *M* coincides with a reflection point *R*. For this situation, the central ray *SRG* is plotted in red and the paraxial ray $\overline{S}R\overline{G}$ is depicted in green.

To obtain reliable information about possible discontinuities in the subsurface, the presence of diffracted waves, in the vicinity of the discontinuity location, is very important. The presence of diffracted waves in the multi-coverage pre-stack seismic data can be useful for detection of discontinuities.

In conventional seismic processing, diffracted waves are regarded as noise and the information contained in these waves has not been used (Landa et al., 1987). In the CRS method, however, attributes can be used to characterize diffraction events.

Finite-Offset (FO) case - In Figure 3 each source point $\overline{S}$ and receiver point $\overline{G}$ are connected with an arbitrary depth point *M*. The sum of both traveltimes from *M* to related source and receivers pairs $\overline{S}, \overline{G}$ defines the diffraction traveltime surface or Huygens surface (Schleicher et al., 1993a). The seismic primary reflections for each pair source-receiver define the reflection time surface. To provide a nonzero contribution for a diffraction stack, both traveltime surfaces (reflection and diffraction) must be tangent if and only if *M=R*, where *R* is the reflection point for each pair *SG*.

According Schleicher et al. (1993a), the 3-D FO diffracted parabolic paraxial traveltime approximation in the vicinity of a FO (central) ray is given by (with a different notation)

$$t_{D,FO}(\mathbf{s},\mathbf{g}) = t_{1,D} - \mathbf{p}_S \cdot \mathbf{s} + \mathbf{p}_G \cdot \mathbf{g} + \frac{1}{2}\left(\mathbf{s}\cdot\mathbf{N}_S^R\mathbf{s} + \mathbf{g}\cdot\mathbf{N}_G^R\mathbf{g}\right), \tag{12}$$

where $t_{1,D}$ is the diffraction traveltime for the central ray *SMG*. The meaning of these quantities, $\mathbf{N}_S^R$ and $\mathbf{N}_G^R$, is analogous to the one explained for formulas (4) to (6).

Squaring equation (12) and retain only its terms up to the second order in **s** and **g**, we obtain

$$t_{D,FO}^2(\mathbf{s},\mathbf{g}) = \left[t_{1,D} - \mathbf{p}_S\cdot\mathbf{s} + \mathbf{p}_G\cdot\mathbf{g}\right]^2 + t_{1,D}\left(\mathbf{s}\cdot\mathbf{N}_S^R\mathbf{s} + \mathbf{g}\cdot\mathbf{N}_G^R\mathbf{g}\right), \tag{13}$$

By considering the relationships, $\mathbf{s} = \mathbf{x}_m - \mathbf{h}$, $\mathbf{g} = \mathbf{x}_m + \mathbf{h}$, and (3) into equation (13), we obtain

$$\begin{aligned} t_{D,FO}^2(\mathbf{x}_m,\mathbf{h}) = {} & \left[t_{1,D} + \mathbf{p}_m\cdot\mathbf{x}_m + \mathbf{p}_h\cdot\mathbf{h}\right]^2 \\ & + t_{1,D}\left[\mathbf{x}_m\cdot\left(\mathbf{N}_S^R + \mathbf{N}_G^R\right)\mathbf{x}_m - \mathbf{x}_m\cdot\left(\mathbf{N}_S^R - \mathbf{N}_G^R\right)\mathbf{h}\right. \\ & \left. - \mathbf{h}\cdot\left(\mathbf{N}_S^R - \mathbf{N}_G^R\right)\mathbf{x}_m + \mathbf{h}\cdot\left(\mathbf{N}_S^R + \mathbf{N}_G^R\right)\mathbf{h}\right] \end{aligned} \tag{14}$$

According to Schleicher et al. (1993a,b) the matrices $\mathbf{N}_S^R$ and $\mathbf{N}_G^R$ are symmetric. By including the relationship followings

$$\mathbf{N}_S^R + \mathbf{N}_G^R = \mathbf{N}_1, \quad \mathbf{N}_S^R - \mathbf{N}_G^R = \mathbf{N}_2, \tag{15}$$

into equation (14) we obtain

$$\begin{aligned} t_{D,FO}^2(\mathbf{x}_m,\mathbf{h}) = {} & \left[t_{1,D} + \mathbf{p}_m\cdot\mathbf{x}_m + \mathbf{p}_h\cdot\mathbf{h}\right]^2 \\ & + t_{1,D}\left[\mathbf{x}_m\cdot\mathbf{N}_1\mathbf{x}_m - \mathbf{x}_m\cdot\mathbf{N}_2\mathbf{h}\right. \\ & \left. - \mathbf{h}\cdot\mathbf{N}_2\mathbf{x}_m + \mathbf{h}\cdot\mathbf{N}_1\mathbf{h}\right], \end{aligned} \tag{16}$$

being this equation (16) the 3-D FO Common-Diffraction-Surface (CDS) stacking operator that depends on ten parameters: two components of vector $\mathbf{p}_m$, two components of vector **h**, three elements of matrix $\mathbf{N}_1$ and three elements of matrix $\mathbf{N}_2$. The matrices $\mathbf{N}_1$ and $\mathbf{N}_2$ are symmetric.

Zero-Offset (ZO) case - In the case of a diffraction point, the 3-D ZO diffracted hyperbolic paraxial traveltime can be formulated by setting the matrices N = M or A = B in equation (9). It yields (Chira et al., 2003)

$$t_{D,ZO}^2(\mathbf{x}_m,\mathbf{h}) = \left(t_0 + \frac{2}{v_1}\mathbf{c}\cdot\mathbf{x}_m\right)^2 + \frac{2t_0}{v_1}\left[\mathbf{x}_m\cdot\mathbf{B}\mathbf{x}_m + \mathbf{h}\cdot\mathbf{B}\mathbf{h}\right], \tag{17}$$

where equation (17) depends on five parameters: three elements of matrix **B** and two components of vector **c**. Equation (17) is called the 3-D ZO CDS stacking operator.

Further applications

Estimation of geometrical spreading factors

For a point source excitation in a 3-D homogeneous medium, a spherical wavefront propagates through the medium without any intrinsic attenuation. The so-called spherical divergence accounts for the amplitude loss that occurs because of the expanding wavefront. The amplitude change is inverse proportional to the radius of curvature of the propagating wavefront. In the case of propagation in an inhomogeneous layered medium, the wavefronts are no longer spherical. Accordingly, the term geometrical spreading (GS) replaces the previously used spherical divergence.

According to ray theory, the GS factor can be accounted for by a factor *L* that appears in denominator of expression of amplitude. The GS is important on the change in amplitude caused by transmission through interfaces along the ray. As a consequence, correct elimination of the GS in the observed amplitudes can be essential for Amplitude versus Offset (AVO) or Amplitude versus Angle (AVA) studies. The term true-amplitude is referred to a section in which the amplitudes have been corrected from their GS effects (Hubral, 1983). In this case, for primary reflections, these amplitudes can be interpreted as (scaled) measures of reflection coefficients, so that AVO or AVA is made possible.

Finite-Offset (FO) case - For a FO (central) ray *SG* the modulus of the normalized geometrical spreading factor is given by (e.g. Hubral et al., 1992b; Hubral et al., 1993)

$$\left|L_{FO}\right| = \frac{\sqrt{\cos a_S \cos a_G}}{v_S}\left|\det \underline{\mathbf{B}}\right|^{1/2}. \qquad (18)$$

Being known the vectores p_S and p_G, we use the following expressions (Tygel et al., 1992)

$$\left|\mathbf{p}_S\right| = \frac{\sin a_S}{v_S}, \quad \text{and} \quad \left|\mathbf{p}_G\right| = \frac{\sin a_G}{v_G}, \qquad (19)$$

to obtain

$$a_S = \arcsin\left(v_S\left|\mathbf{p}_S\right|\right), \quad \text{and} \quad a_G = \arcsin\left(v_G\left|\mathbf{p}_G\right|\right). \qquad (20)$$

Zero-Offset (ZO) case - For this case, the 3-D GS factor L_{ZO} can be expressed as (Hubral, 1983)

$$L_{ZO} = \frac{2}{\sqrt{\det(\mathbf{M}-\mathbf{N})}}. \qquad (21)$$

Introducing equations (10) into equation (21), we find that L_{ZO} can be recast as

$$L_{ZO} = \frac{2}{\sqrt{\det(\mathbf{D}_{zy}^T\mathbf{B}\mathbf{D}_{zy} - \mathbf{D}_{zy}^T\mathbf{A}\mathbf{D}_{zy})}}. \qquad (22)$$

Projected Fresnel zones

The concept of a projected Fresnel zone was introduced for ZO reflections (Hubral et al., 1993) and extended to arbitrary FO rays by Schleicher et al. (1997). The projected Fresnel zone is defined as the region on the earth surface or on the reflection traveltime surface that contains the events reflected from the actual Fresnel zone on the reflector along the pertinent rays corresponding to the measurement configuration (Schleicher et al. 2003). This zone plays an important role in diffraction-stack (or Kirchhoff) migration in connection with the migration aperture, i.e. the number of traces that are summed up along diffraction time surfaces. The projected Fresnel zone corresponds to the minimum migration aperture that is needed to guarantee correctly recovered migration amplitudes together with the best S/N ratio (Schleicher et al. 2003).

The projected Fresnel zone also represents an optimum aperture for the stacking procedure. It was applied successfully for the 3-D ZO CRS stack (e.g. Cristini et al. 2001, Cristini et al. 2002, Bergler et al. 2002).

Finite-Offset (FO) case - For the 3-D FO CRS stacking operator (equation 2), the projected Fresnel zone matrix is given by (Schleicher et al. 1997)

$$\mathbf{H}_p^{FO} = \mathrm{L}^T\mathbf{H}^{-1}\mathrm{L}, \qquad (23)$$

where (see e.g. Hubral et al. 1992b; Hubral et al., 1993)

$$\mathrm{L} = \mathbf{B}_2^{-1}\mathrm{G}_G + \mathbf{B}_1^{-T}\mathrm{G}_S, \qquad (24)$$

$$\mathbf{H} = \mathbf{D}_1\mathbf{B}_1^{-1} + \mathbf{B}_2^{-1}\mathbf{A}_2 = \mathbf{B}_2^{-1}\underline{\mathbf{B}}\mathbf{B}_1^{-1}, \qquad (25)$$

being the symmetric Fresnel zone matrix represented by **H**. The matrices $\mathrm{G_S}$ and $\mathrm{G_G}$ are called the configuration matrices (Schleicher et al. 1993b).

For different configurations the values of matrices $\mathrm{G_S}$ and $\mathrm{G_G}$ (Schleicher et al. 1993b) are substituted into equation (23) to obtain different forms of the projected Fresnel zone matrix .

•Common-shot (CS) gather - The configuration matrices are defined as $\mathrm{G_S}$ = **0** and $\mathrm{G_G}$ = **I**. We substitute these conditions into equation (23) to obtain

$$\mathbf{H}_p^{CS} = \mathbf{B}_2^{-T}\left(\mathbf{D}_1\mathbf{B}_1^{-1} + \mathbf{B}_2^{-1}\mathbf{A}_2\right)^{-1}\mathbf{B}_2^{-1}. \qquad (26)$$

•Common-receiver (CR) gather- The configuration matrices are defined as $\mathrm{G_S}$ = **I** and $\mathrm{G_G}$ = **0**. We substitute these conditions into equation (23) to obtain

$$\mathbf{H}_p^{CR} = \mathbf{B}_1^{-T}\left(\mathbf{D}_1\mathbf{B}_1^{-1} + \mathbf{B}_2^{-1}\mathbf{A}_2\right)^{-1}\mathbf{B}_2^{-1}. \qquad (27)$$

•Common-offset (CO) gather- In this case, the configuration matrices are defined as $\mathrm{G_S}$ = **I** and $\mathrm{G_G}$ = **I**. We substitute these conditions into equation (23) to obtain

$$\mathbf{H}_p^{CO} = \left(\mathbf{B}_2^{-1} + \mathbf{B}_1^{-T}\right)^T\left(\mathbf{D}_1\mathbf{B}_1^{-1} + \mathbf{B}_2^{-1}\mathbf{A}_2\right)^{-1}\left(\mathbf{B}_2^{-1} + \mathbf{B}_1^{-T}\right). \qquad (28)$$

•Zero-Offset (FO) case - For the 3-D ZO CRS stacking operator (equation 7), the projected Fresnel zone on the earth surface expressed by (Hubral et al., 1993)

$$\left|\mathbf{x}_P \cdot \mathbf{H}_p^{ZO}\mathbf{x}_P\right| \le t, \qquad (29)$$

where the vector $\mathbf{x}_P$ is the projected coordinate into the earth surface of a point in the vicinity of NIP on the reflector (Hubral et al., 1993). The period of the considered time-harmonic wave is given by τ. Following Hubral et al. (1993) the projected Fresnel matrix $\mathbf{H}_p$ is given by

$$\mathbf{H}_p^{ZO} = 32\left(\mathbf{B}_0^{-1}\mathbf{A}_0 - \mathbf{D}_0^{-1}\mathbf{C}_0\right). \qquad (30)$$

Introducing the relationships for the 3-D ZO CRS stacking operator, $\mathbf{D}_0^{-1}\mathbf{C}_0 = \mathbf{A}/v_1$ and $\mathbf{B}_0^{-1}\mathbf{A}_0 = \mathbf{B}/v_1$ (Chira, 2003) into equation (30) we obtain (Chira et al., 2003)

$$\mathbf{H}_p^{ZO} = \frac{32}{v_1}\left(\mathbf{B} - \mathbf{A}\right). \qquad (31)$$

Finally, we include (31) into equation (29) to obtain

$$\frac{32}{v_1}\left|\mathbf{x}_P \cdot \left[\mathbf{B}-\mathbf{A}\right]\mathbf{x}_P\right| \le t, \qquad (32)$$

Equation (32) can be considered as the initial aperture for the 3-D ZO CRS stacking operator (equation 9).

Conclusions

We present the formalism and examples of applications of the 3-D CRS stacking operator for reflection events. This operator depends on fourteen search-parameters for the FO case and eight search-parameters for the ZO case. We provide the 3-D CRS stacking operators for diffraction events which depends on ten parameters for the FO case and five parameters for the ZO case. These stacking operators are in fact valid for a 3-D laterally inhomogeneous velocity model and can be used to simulate FO or ZO volumes from multi-coverage prestack seismic dataset. We also show special formulas for applications of the 3-D CRS attributes to determine the geometrical spreading factors and Projected Fresnel zones. These latter applications are important to define the aperture for stacking and migration.

Acknowledgments

The first author thanks to National Council of Technology and Development (CNPq) for the scholarship.

References

Bergler, S., Hubral, P., Marchetti, P. Cristini, A. and Cardone, G., 2002. 3D common-reflection-surface stack and kinematic wavefield attributes. The Leading Edge, 21, p. 1010-1015.

Bortfeld, R., 1989. Geometrical ray theory: Rays and traveltimes in seismic systems (second order approximation of the traveltimes). Geophysics,1(54), p. 342-349.

Cardone, G., Cristini, C., Bonomi, A., Marchetti, P., Zambonini, R., Hubral, P. and Mann, J., 2003. 3D zero-offset CRS for narrow-azimuth data: formulation and examples. In EAGE/SEG Summer Research Workshop on processing and imaging of seismic data - using explicit or implicit velocity model information? EAGE. Expanded Abstract, Sesion T006.

Chira-Oliva, P., Cruz, J. C. R., Hubral, P. and Tygel, M., 2003. Theoretical aspects of the 3-D ZO CRS stack. 8th International Congress of the SBGf, BRAZIL.

Chira, P., 2003. Empilhamento pelo método Superfície de Reflexão Comum 2-D com Topografia e Introdução ao caso 3-D in portuguese. Ph.D. Thesis, Federal University of Para, Brazil.

Cristini, A., Cardone, G., Chira, P. Hubral, P. and Marchetti, P., 2001. 3D Zero-Offset Common Reflection Surface Stack for Land Data. 46th Annual Internat. Mtg., Soc. Expl. Geophys., Expanded Abstracts, Session W5-13.

Cristini, A., Cardone, G., Marchetti, P., 2002. 3D Zero-Offset Common Reflection Surface Stack for land data - real data example. Expanded Abstract of the 64th EAGE Conference and Technical Exhibition, Sesion B15.

Cristini, A. Cardone, G., Marchetti, P. and Zambonini, R., 2003. 3D ZO CRS Stack: issues related to complex structures and real data. 73rd Annual Internat. Mtg., Soc. Expl. Geophys., Expanded Abstracts.

Garabito, G., Cruz, J. C. R., Hubral, P. and Costa, J., 2001. Common reflection surface stack: A new parameter search strategy by global optimization. 71th. SEG Mtg., Expanded Abstracts. San Antonio, Texas,USA.

Hubral, P., Tygel, M. and Zien, H., 1991. Three-dimensional true-amplitude zero-offset migration. Geophysics, 56(1), p. 18-26.

Hubral, P., Schleicher, J. and Tygel, M., 1992a. Three-dimensional paraxial ray properties, Part I: Basic relations. Journal of Seismic Exploration, 1, p. 265-279.

Hubral, P. Schleicher, J. and Tygel, M., 1992b. Three-dimensional paraxial ray properties, Part II: Applications. Journal of Seismic Exploration, 1, p. 347-362.

Hubral, P., Schleicher, J. Tygel, M. and Hanitzsch, C., 1993. Determination of Fresnel zones and traveltimes measurement. Geophysics, 58, p. 703-712.

Hubral, P., 1983. Computing true amplitude reflections in a laterally inhomogeneous earth. Geophysics, 48, p. 1051-1062.

Hubral, P., 1999. Macro-model independent seismic reflection imaging. J. Appl. Geoph., 42, nos. 3,4.

Jäger, R. Mann, J. Höcht, G. Hubral, P., 2001. Common Reflection Surface Stack: Image and Attributes. Geophysics,66, p. 97-109.

Jäger, R., 1999. The Common-Reflection surface stack - Theory and application. Master's thesis. University of Karlsruhe, Germany.

Landa, E., Shtivelman, V. and Gelchinsky, G., 1987. A method for detection of diffracted waves on common-offset sections. Geophysical Prospecting, 35, p. 359-373.

Mann, J. Jäger, R., Müller, T. Höcht, G. and Hubral, P., 1999. Common-reflection-surface stack - A real data example. Journal of Applied Geophysics, 42, 301-318.

Schleicher, J., Tygel, M. and Hubral, P., 1993a. Parabolic and hyperbolic paraxial two-point traveltimes in 3D media. Geophysical Prospecting, 41(4), p. 495-514.

Schleicher, J., Tygel, M. and Hubral, P., 1993b. 3-D true-amplitude finite-offset migration. Geophysics, 58(8), p. 1112-1126.

Schleicher, J., Hubral, P. Tygel, M. and Jaya, M., 1997. Minimum apertures and Fresnel zones in migration and demigration, Geophysics, 62(1), p. 183-194.

Schleicher, J., Tygel, M. and Hubral, P., 2003. Seismic true emplitude imaging. SEG monograph in press.

Tygel, M., Schleicher, J. and Hubral, P., 1992. Geometrical spreading corrections of offset reflections in a laterally inhomogeneous earth. Geophysics, 57(8), 1054-1063.